

# Terahertz emission from laser-induced microplasma in ambient air

FABRIZIO BUCCHERI AND XI-CHENG ZHANG\*

The Institute of Optics, University of Rochester, 275 Hutchison Road, Rochester, New York 14627, USA

\*Corresponding author: xi-cheng.zhang@rochester.edu

Received 5 January 2015; revised 13 February 2015; accepted 23 March 2015 (Doc. ID 231464); published 9 April 2015

**The integration of ambient air plasmas as source and sensor in terahertz time-domain techniques allows spectral measurements covering the elusive terahertz gap (0.1–10 THz), further increasing the impact of those scientific tools in the study of the four states of matter. In this article we describe the experimental study of the terahertz emission from a laser-induced plasma of submillimeter size. The main direction of emission is almost orthogonal to the laser propagation direction, unlike that of elongated plasmas. We show that laser pulse energies lower than 1  $\mu\text{J}$  are sufficient to generate measurable terahertz pulses from ambient air. This significant decrease in the required laser energy will make plasma-based terahertz techniques more accessible to the scientific community.** © 2015 Optical Society of America

**OCIS codes:** (260.5210) Photoionization; (300.6495) Spectroscopy, terahertz; (320.7110) Ultrafast nonlinear optics; (350.5400) Plasmas.

<http://dx.doi.org/10.1364/OPTICA.2.000366>

Terahertz (THz) time-domain techniques, such as time-resolved THz spectroscopy (TRTS) [1] and THz time-domain spectroscopy (THz-TDS) [2], are becoming widely used tools to study the dynamics and equilibrium properties of the four states of matter [3–6].

In most studies those techniques were implemented using solid-state THz emitters and sensors, specifically inorganic nonlinear crystals or photoconductive antennas, which limited the spectral coverage of the measurements to a few THz. However, the ability to access a broader portion of the electromagnetic spectrum extending to higher frequencies is in demand. In fact, for nonequilibrium studies, it allows simultaneous access to correlated dynamics associated with different excitation channels having spectral signatures in separate frequency regions. An example is given in [7], which analyzed the evolution of phonon features and electron conductivity during a photoinduced phase transition in  $\text{VO}_2$ . Moreover, from an application standpoint, one should consider the presence of THz spectral signatures in chemicals relevant to security applications, e.g., explosives and drugs, across the entire THz gap [8,9]. Therefore, being able to cover an extended spectral range improves the confidence with which those

substances can be identified by increasing the number of their spectral “fingerprints” within the measurement window.

The spectral coverage of THz time-domain techniques can be significantly increased by using gas plasmas induced by energetic femtosecond pulses as both THz source and sensor [10–14]. Another approach worth mentioning is the use of thin electro-optic organic polymers [15]. However, with gas plasmas there is no concern about laser-induced damage at high intensities. Moreover, gas plasmas provide a gradual refractive index interface to the THz radiation, as opposed to the abrupt interface of a solid material, therefore eliminating the spectral spatial filtering due to total internal reflection and the introduction of Fresnel reflections in the measurements.

The first report of THz generation from ionized gas is attributed to Hamster *et al.* in 1993 [16]. In their experiment, 50 mJ near-infrared pulses were tightly focused on He gas targets resulting in the measurement of subpicosecond transients with optical to THz conversion efficiency of less than  $10^{-6}$ . However, it was later shown by Cook and Hochstrasser that the conversion efficiency can be improved to  $10^{-5}$ – $10^{-4}$  when the medium is ionized by an ultrafast laser field composed by the fundamental and its second harmonic [17]. The two different techniques are usually referred to as the “one-color” and “two-color” approaches, respectively.

In the majority of cases, both techniques are implemented by focusing the laser field with numerical apertures (NAs) smaller than 0.2, resulting in the creation of elongated plasma strings for which the longitudinal dimension is much greater than the transverse one. Typical lengths for those elongated plasmas range from a few millimeters to tens of centimeters.

Regarding the choice of gas to be used, it is remarkable that ambient air itself, employed as an intense THz source and ultra-broadband sensor, allows the realization of spectroscopic measurements with high signal-to-noise ratio (SNR) and dynamic range [11–14,18]. Despite other gases offering improved performance in terms of generation efficiency [19] and detection sensitivity [20], ambient air is readily available, does not require the use of a gas cell, and clearly does not impose any health hazard or handling complexity.

However, the requirement for the air to be ionized together with the use of low-NA focusing limits the realization of THz plasma sources with low repetition rate amplified ultrafast laser systems (with millijoule pulse energies). Hence, compared to

solid-state emitters, cost and complexity are moved from the THz source to the laser system. Throughout the manuscript we will refer to the minimum value of laser pulse energy necessary to generate measurable THz waveforms as the laser energy threshold. Reported values in literature for this quantity are in the range of 30–50  $\mu\text{J}$  [21,22].

In this Letter we demonstrate the use of ambient air laser-induced microplasmas as THz emitters. For these sources the laser energy threshold is reduced to the submicrojoule level. Other features of interest are that the THz waves are radiated almost orthogonally to the laser propagation direction, and that the generation volume is subwavelength compared to the emission wavelength (1 THz = 300  $\mu\text{m}$ ).

Our study is limited to the one-color approach. Under this condition the emission of THz transients is attributed to space charge separation induced by the ponderomotive forces located in the proximity of the focal plane [16,23]. The following estimate scaling law for the THz peak power  $P_{\text{THz}}$  as a function of the relevant laser source parameters has been proposed by Hamster *et al.* [23]:

$$P_{\text{THz}} \propto \frac{(W \cdot \text{NA} \cdot \lambda)^2}{\tau^4}, \quad (1)$$

where  $W$  is the laser pulse energy, NA is the numerical aperture of the focusing laser cone,  $\lambda$  is the laser wavelength, and  $\tau$  is the pulse duration. This simple analysis does not rigorously take into account all of the phenomena that may affect the THz generation process and its validity has not been tested experimentally; however, it provides an interesting insight. In fact, it suggests that a tight focusing geometry with high-NA optics allows both decreasing the laser energy threshold, by increasing the laser intensity at the focal plane, and improving the THz generation efficiency. Indeed, our experimental approach was to maximize the ponderomotive force by focusing the laser field with high-NA optics, leading to estimated peak intensities at the focal point exceeding  $10^{14} \text{ W/cm}^2$  and a very steep intensity gradient around the focal volume.

Our experimental setup implemented THz time-resolved detection, and it is schematically shown in Fig. 1. The laser excitation, provided by a commercial Ti:sapphire amplified laser (100 fs pulse duration, 700  $\mu\text{J}$  pulse energy, 800 nm central wavelength, 1 kHz repetition rate), was split into two beams with controllable time delay (not shown in the figure).

The pump beam was focused by a 0.85 NA air-immersion microscope objective into ambient air, creating a submillimeter plasma. The polarization of the pump beam was linear, and its orientation could be rotated through a half-wave plate. The maximum pump pulse energy employed in the experiment was 65  $\mu\text{J}$ , limited by the damage threshold of the objective. For this excitation energy we obtained plasmas with both longitudinal and transverse sizes less than 40  $\mu\text{m}$  (Fig. 1 inset). THz field resolved traces were obtained through free-space electro-optic sampling [24], where we employed a 3 mm thick (110)-cut ZnTe crystal as the detector.

In order to study the angle-dependent emission of the source, the pump section was installed on a platform able to rotate about the geometrical focus of the microscope objective. We implemented a design that minimized the optical path difference between the pump and probe arms upon rotation, so to reduce the user intervention and the experimental error.

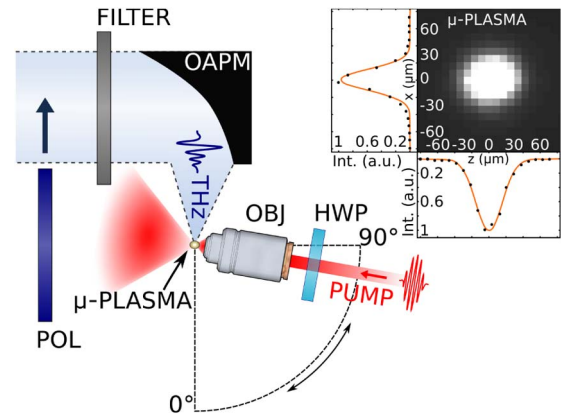


**Fig. 1.** THz waves are emitted by the ambient air microplasma obtained by focusing the laser excitation through a high-NA objective. A silicon wafer is inserted in the THz path to block the pump beam. The waveforms are retrieved with electro-optic sampling. The THz generation portion of the setup can be rotated about the position of the microplasma in order to study the angle-dependent emission from the source. The inset is a picture of the microplasma created by focusing laser pulses with energy of 65  $\mu\text{J}$  through a 0.85 NA air-immersion objective as seen through a UV bandpass filter. The laser excitation propagates from right to left. The plasma is imaged from the side with a commercial iCCD camera. The fluorescence profile is Gaussian. The FWHM for the longitudinal and the transverse fluorescence intensity profile is  $36.7 \pm 8.7 \mu\text{m}$  and  $28.5 \pm 8.7 \mu\text{m}$ , respectively. HWP, half-wave plate; OBJ, objective; OAPM, off-axis parabolic mirror; POL, THz polarizer.

Our findings are illustrated in Fig. 2. We measured THz waveforms for 10 different detection angles, defined as the angle between the propagation axis of the pump beam and the optical axis of the THz collecting mirror, ranging from 0 to 90 deg. The solid angle of collection was limited by the diameter of the first off-axis parabolic mirror for all detection angles. Figure 2(a) shows the time-resolved field measurements, while Fig. 2(b) (solid line) depicts the collected THz pulse energy, extracted from the field measurements, as a function of detection angle. In our experimental conditions, the coherent emission of THz collected in the forward direction, 0 deg, is negligible compared to the one collected for detection angles close to 90 deg. Specifically, we observed the peak of THz emission to occur around 80 deg.

A typical THz waveform measured for this value of detection angle for laser pulse energy of 65  $\mu\text{J}$  is shown in Fig. 3(a) (top waveform). The detected spectrum is broadband, as shown in Fig. 3(b), and it is limited by the useful detection bandwidth, which is related to the electro-optic crystal thickness and phonon resonances.

We also report the measurement of THz emission from ambient air excited with submicrojoule laser pulse energies. For these low levels of energy we were not able to detect any fluorescence emission from the microplasma using the iCCD camera. Figure 3 shows a THz waveform recorded for pump energy as low as 660 nJ (bottom waveform). This value is more than 1 order of magnitude lower than previously reported ones [21,22] and it is limited by the SNR of the detection system.

A simple strategy to improve the SNR significantly is to use laser sources with higher repetition rate, resulting in an increased number of measured pulses in the unit of time. Commercial amplified laser systems with pulse energies of few microjoules typically have repetition rates of the order of 200–300 kHz, which

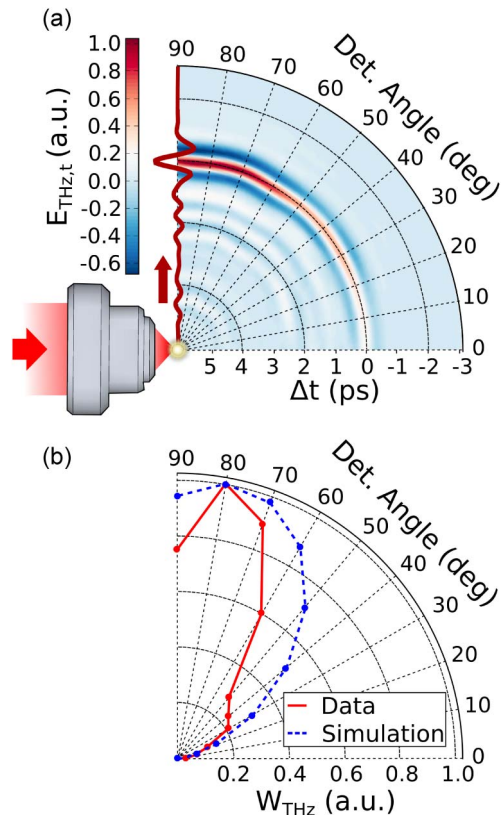


**Fig. 2.** (a) Density plot representing the coherent angle-dependent emission from a microplasma generated with laser pulse energy of 65  $\mu\text{J}$ . The plot is obtained through spline interpolation of ten THz waveforms recorded at different detection angles in 10 deg intervals starting from zero. Each waveform is normalized to the highest value of THz field recorded in the set.  $\Delta t$  is the time delay between the pump and the probe beam. (b) THz pulse energy as a function of detection angle. The pulse energy is extracted from the THz waveforms displayed in (a). The solid line is the experimental data, while the dashed line is the simulation obtained with the model described in [29].

is an increase of 2 orders of magnitude compared to the repetition rate of our laser system. Considering that the SNR is expected to grow as the square root of the repetition rate, by employing this class of sources we expect the SNR to be improved by more than 1 order of magnitude, and THz transients to be measured with even lower pulse energies.

Consistent with Eq. (1), the THz peak power scales with the square of the pump pulse energy, as shown in Fig. 4, independently of detection angle. For pump pulse energies above 55  $\mu\text{J}$ , the experimental data starts to deviate from the parabolic fit. We are not able to discriminate whether this is due to the saturation of the THz emission mechanism, or to nonlinear interactions between the intense laser pulse and the glass composing the objective, such as self-phase modulation.

The measured THz emission pattern, amplitude, and phase are not sensitive to linear polarization rotations of the optical pump. Furthermore, we investigated the polarization of the detected THz radiation by inserting a wire grid polarizer in the THz path (see Fig. 1), and exploiting the inherent polarization sensitivity of electro-optic sampling similarly to [25]. THz radiation within our collection angle was horizontally polarized independently of the pump beam polarization. Due to the cylindrical

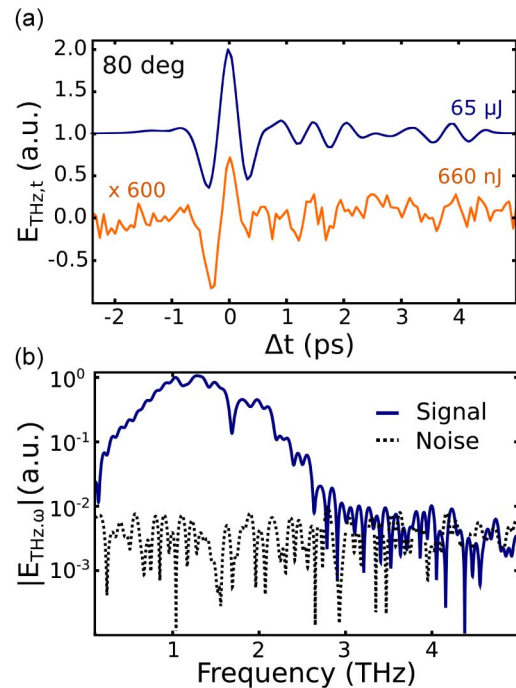


**Fig. 3.** (a) Measured THz waveforms at detection angle of 80 deg for a laser pulse energy of 65  $\mu\text{J}$  (top) and of 660 nJ (bottom). For clarity, the plots are offset and the waveform measured at 660 nJ is magnified 600 times. (b) Spectral amplitude of the THz waveform measured at detection angle of 80 deg for a laser pulse energy of 65  $\mu\text{J}$  (solid line), and of the noise at the detector (dashed line).

symmetry of the generation mechanism, this implies that the THz emission is locally linearly polarized, and oscillating in the plane defined by the laser excitation propagation axis and the local THz propagation axis.

The radiation pattern from the microplasma source is significantly different from that of elongated plasmas. The main direction of radiation is, in fact, almost orthogonal to the laser propagation and spatially separated from the laser excitation beam. Conversely, for elongated plasmas, both in the one-color and two-color approaches, despite very different generation mechanisms, it was shown that THz is emitted as a forward propagating cone whose divergence angle increases as the length of the plasma string decreases [26–28].

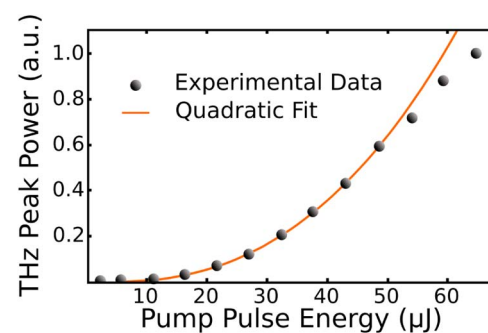


**Fig. 4.** THz peak power as a function of laser pulse energy for a detection angle of 80 deg. The dots are the experimental data, while the solid line is a quadratic fit.

The experimental findings in condition of high-NA focusing are all consistent with the interpretation of THz emission from one-color plasma given by Hamster *et al.* [16,23]. Coherent THz radiation originates from plasma currents driven by the laser ponderomotive force. This force is proportional to the local intensity gradient, and, therefore, it is not strongly affected by polarization rotations of the linearly polarized laser field. The measured radiation pattern in Fig. 2(b), whose peak is almost orthogonal to the laser propagation direction, suggests that THz radiation originates from longitudinal plasma currents.

Remarkably, the 1D analytical model proposed to explain the forward THz emission from filaments within the framework of transition-Cherenkov-like emission described in [29] would also qualitatively describe the radiation pattern when the length of the filament is reduced to 40  $\mu\text{m}$ , as shown in Fig. 2(b).

The THz emission is calculated as the far-field radiation of a longitudinal plasma current  $j_z(\omega)$ . The energy spectral density emitted in the unit solid angle is [29]

$$\frac{d^2 W_{\text{THz}}}{d\omega d\Omega} \propto |j_z(\omega)|^2 f(\omega, \theta, L), \quad (2)$$

$$f(\omega, \theta, L) = \frac{\sin^2 \theta}{(1 - \cos \theta)^2} \sin^2 \left( \frac{L\omega}{2c} (1 - \cos \theta) \right), \quad (3)$$

where  $\theta$  is the emission angle,  $L$  is the longitudinal length of the plasma column, and  $c$  is the speed of light.

To compare the model to our experimental results, for each value of detection angle we numerically integrated Eq. (2) over the frequency interval accessible with our detection technique (0.1–2.5 THz) and over the detection solid angle. For our experimental conditions we estimated the electron densities to be greater than  $10^{18} \text{ cm}^{-3}$ , corresponding to plasma frequencies higher than 9 THz, and electron collision frequencies much smaller than the plasma frequency. As shown in Fig. 2(b), this simple analysis correctly predicts the angle of maximum emission, although it yields a less directive radiation pattern compared to the experimental data.

The radiation pattern is mainly described by the geometrical factor  $f(\omega, \theta, L)$ , which describes the far-field summation of radiation coming from a source moving at the speed of light over a finite length  $L$ , and it is loosely affected by the spectral content of the excitation current  $j_z(\omega)$ .

The emission from the microplasma can be intuitively visualized as the emission from a dipole antenna, which is characterized by the presence of two lobes oriented orthogonally to its axis. In the microplasma, however, the current is not fed externally, but it is due to an effective dipole created behind the ionization front of the laser excitation. This dipole-like source moves at the group velocity of the optical pulse over a finite length, causing the lobes not to be exactly orthogonal to the laser propagation direction. The coherent nature of the emission suggests that more complicated, even arbitrary, radiation patterns might be achieved by combining the radiation from multiple microplasmas, similarly to a phase array.

In conclusion, we demonstrated the use of laser-induced microplasmas as a broadband THz wave source. We measured THz waveforms generated with laser pulse energies as low as 660 nJ. Further optimization of the technique, including improved design of the THz collection optics, the use of the two-color

approach, of longer excitation laser wavelengths and shorter pulse durations, has the promise to tap the full potential of plasma-based THz techniques with low-energy ultrafast lasers.

Moreover, the combination of a radiation pattern where the THz emission is spatially separated from the laser excitation and of a subwavelength source size (1 THz = 300  $\mu\text{m}$ ) might promote new applications, such as plasma-based THz near-field techniques.

Army Research Office (ARO) (W911NF-14-1-0343); National Science Foundation (NSF) (ECCS-1229968).

We wish to thank Prof. B. Bousquet, Prof. P. Mounaix, Prof. S. Skupin, and Prof. J. Dai for useful discussions.

## REFERENCES

1. M. Nuss, D. Auston, and F. Capasso, *Phys. Rev. Lett.* **58**, 2355 (1987).
2. M. van Exter, C. Fattinger, and D. Grischkowsky, *Opt. Lett.* **14**, 1128 (1989).
3. B. H. Kolner, R. A. Buckles, P. M. Conklin, and R. P. Scott, *IEEE J. Sel. Top. Quantum Electron.* **14**, 505 (2008).
4. P. U. Jepsen, D. G. Cooke, and M. Koch, *Laser Photon. Rev.* **5**, 124 (2011).
5. R. Ulbricht, E. Hendry, J. Shan, T. F. Heinz, and M. Bonn, *Rev. Mod. Phys.* **83**, 543 (2011).
6. A. I. McIntosh, B. Yang, S. M. Goldup, M. Watkinson, and R. S. Donnan, *Chem. Soc. Rev.* **41**, 2072 (2012).
7. C. Kübler, H. Ehrke, R. Huber, R. Lopez, A. Halabica, R. Haglund, and A. Leitenstorfer, *Phys. Rev. Lett.* **99**, 116401 (2007).
8. M. R. Leahy-Hoppa, M. J. Fitch, X. Zheng, L. M. Hayden, and R. Osiander, *Chem. Phys. Lett.* **434**, 227 (2007).
9. A. G. Davies, A. D. Burnett, W. Fan, E. H. Linfield, and J. E. Cunningham, *Mater. Today* **11**(3), 18 (2008).
10. J. Dai, X. Xie, and X.-C. Zhang, *Phys. Rev. Lett.* **97**, 103903 (2006).
11. N. Karpowicz, J. Dai, X. Lu, Y. Chen, M. Yamaguchi, H. Zhao, X.-C. Zhang, L. Zhang, C. Zhang, M. Price-Gallagher, C. Fletcher, O. Mamer, A. Lesimple, and K. Johnson, *Appl. Phys. Lett.* **92**, 011131 (2008).
12. J. Liu and X. C. Zhang, *J. Appl. Phys.* **106**, 023107 (2009).
13. M. Zalkovskij, C. Zoffmann Bisgaard, A. Novitsky, R. Malureanu, D. Savastru, A. Popescu, P. Uhd Jepsen, and A. V. Lavrinenko, *Appl. Phys. Lett.* **100**, 031901 (2012).
14. F. D'Angelo, Z. Mics, M. Bonn, and D. Turchinovich, *Opt. Express* **22**, 12475 (2014).
15. C. V. McLaughlin, L. M. Hayden, B. Polishak, S. Huang, J. Luo, T.-D. Kim, and A. K.-Y. Jen, *Appl. Phys. Lett.* **92**, 151107 (2008).
16. H. Hamster, A. Sullivan, S. Gordon, W. White, and R. Falcone, *Phys. Rev. Lett.* **71**, 2725 (1993).
17. D. J. Cook and R. M. Hochstrasser, *Opt. Lett.* **25**, 1210 (2000).
18. B. Clough, J. Dai, and X.-C. Zhang, *Mater. Today* **15**(1–2), 50 (2012).
19. Y. Chen, M. Yamaguchi, M. Wang, and X.-C. Zhang, *Appl. Phys. Lett.* **91**, 251116 (2007).
20. X. Lu, N. Karpowicz, Y. Chen, and X.-C. Zhang, *Appl. Phys. Lett.* **93**, 261106 (2008).
21. M. Kress, T. Löffler, S. Eden, M. Thomson, and H. G. Roskos, *Opt. Lett.* **29**, 1120 (2004).
22. X. Xie, J. Dai, and X.-C. Zhang, *Phys. Rev. Lett.* **96**, 075005 (2006).
23. H. Hamster, A. Sullivan, S. Gordon, and R. Falcone, *Phys. Rev. E* **49**, 671 (1994).
24. Q. Wu and X.-C. Zhang, *Appl. Phys. Lett.* **67**, 3523 (1995).
25. M. Sato, T. Higuchi, N. Kanda, K. Konishi, K. Yoshioka, T. Suzuki, K. Misawa, and M. Kuwata-Gonokami, *Nat. Photonics* **7**, 724 (2013).
26. C. D'Amico, A. Houard, M. Franco, B. Prade, A. Mysyrowicz, A. Couairon, and V. Tikhonchuk, *Phys. Rev. Lett.* **98**, 235002 (2007).
27. H. Zhong, N. Karpowicz, and X.-C. Zhang, *Appl. Phys. Lett.* **88**, 261103 (2006).
28. Y. S. You, T. I. Oh, and K. Y. Kim, *Phys. Rev. Lett.* **109**, 183902 (2012).
29. C. D'Amico, A. Houard, S. Akturk, Y. Liu, J. Le Bloas, M. Franco, B. Prade, A. Couairon, V. T. Tikhonchuk, and A. Mysyrowicz, *New J. Phys.* **10**, 013015 (2008).